Spectral density mapping protocols for analysis of molecular motions in disordered proteins

ARTICLE *in* JOURNAL OF BIOMOLECULAR NMR · FEBRUARY 2014

Impact Factor: 3.14 · DOI: 10.1007/s10858-014-9816-4 · Source: PubMed

6 AUTHORS, INCLUDING:

Libor Krásný
Institute of Microbiology, Academy of Scien…
32 PUBLICATIONS **437** CITATIONS
SEE PROFILE

Vladimír Sklenář
Masaryk University
154 PUBLICATIONS **7,562** CITATIONS
SEE PROFILE

J Biomol NMR (2014) 58:193–207
DOI 10.1007/s10858-014-9816-4

ARTICLE

Spectral density mapping protocols for analysis of molecular motions in disordered proteins

Pavel Kadeřávek · Vojtěch Zapletal · Alžbeta Rabatinová · Libor Krásný · Vladimír Sklenář · Lukáš Žídek

Received: 11 October 2013 / Accepted: 28 January 2014 / Published online: 11 February 2014

Abstract Spectral density mapping represents the method of choice for investigations of molecular motions of intrinsically disordered proteins (IDPs). However, the current methodology has been developed for well-folded proteins. In order to find conditions for a reliable analysis of relaxation of IDPs, accuracy of the current reduced spectral density mapping protocols applied to IDPs was examined and new spectral density mapping methods employing cross-correlated relaxation rates have been designed. Various sources of possible systematic errors were analyzed theoretically and the presented approaches were tested on a partially disordered protein, delta subunit of bacterial RNA polymerase. Results showed that the proposed protocols provide unbiased description of molecular motions of IDPs and allow to separate slow exchange from fast dynamics.

Keywords Nuclear magnetic resonance · Relaxation · Spectral density function · Intrinsically disordered proteins

Electronic supplementary material The online version of this article (doi:10.1007/s10858-014-9816-4) contains supplementary material, which is available to authorized users.

P. Kadeřávek · V. Zapletal · V. Sklenář · L. Žídek (✉)
Central European Institute of Technology, Masaryk University, Kamenice 5, 625 00 Brno, Czech Republic
e-mail: lzidek@chemi.muni.cz

P. Kadeřávek · V. Zapletal · V. Sklenář · L. Žídek
National Centre for Biomolecular Research, Faculty of Science, Masaryk University, Kamenice 5, 625 00 Brno, Czech Republic

A. Rabatinová · L. Krásný
Institute of Microbiology, Academy of Sciences of the Czech Republic, Vídeňská 1083, 142 00 Prague 4, Krč, Czech Republic

Introduction

The finding that unstructured polypeptide chains do not necessary represent a failure of the protein expression machinery but may play important biological roles initiated a new era in protein chemistry (Tompa 2012; Uversky 2013). Transient structural motifs of the intrinsically disordered proteins (IDPs) have been studied in a great detail by various techniques, among which nuclear magnetic resonance (NMR) plays a prominent role (Dyson and Wright 2004; Eliezer 2007, 2009). Knowledge of internal dynamics, contributing to the understanding of a function of any protein, is even more important in the case of the highly flexible IDPs.

NMR relaxation provides a valuable insight into molecular motions of both ordered and disordered proteins. However, interpretation of the relaxation data of IDPs have to take into account the lack of a regular structure. The assumption of a statistical independence of global and local motions, the corner-stone of the most popular *model-free* analysis of dynamics of well-ordered proteins (Lipari and Szabo 1982a, b; Halle et al. 1981), is obviously not valid for IDPs. Therefore, a conservative approach that relies on a very little prior knowledge of the motions, known as the *spectral density mapping*, represents a method of choice for NMR motional studies of IDPs (Farrow et al. 1997; Ochsenbein et al. 2001; Bussell and Eliezer 2001; Yao et al. 2001; Cao et al. 2004; Zhang et al. 2005).

The basic principles of the spectral density mapping are well established and described in the literature (Peng and Wagner 1992a, b). The semi-classical NMR relaxation theory (Wangsness and Bloch 1953; Redfield 1965) shows that the relaxation rates are given by linear combinations of discrete values of the real part of the Fourier transformed time correlation function, known as *spectral density*

function $J(\omega)$. The relevant values of $J(\omega)$ are given by the particular characteristic frequencies, defined by the magnetic field and relaxation mechanism.

The most reliable relaxation rates are obtained for ^{15}N nuclei in the backbone amide group of ^{15}N-labeled proteins, which can be treated as an isolated ^{15}N–^{1}H spin pair. In such a case, only two mechanisms significantly contribute to the ^{15}N relaxation, namely chemical shift anisotropy of ^{15}N and dipole–dipole interaction between ^{15}N and ^{1}H. Moreover, the chemical shift tensor of ^{15}N is almost axially symmetric, with the main axis deviating only slightly from the direction of the ^{15}N–^{1}H bond (Korzhnev et al. 2001). This geometry allows to describe both relaxation mechanisms by the same spectral density function without introducing a large error. Finally, the number of characteristic frequencies of the ^{15}N–^{1}H interaction can be reduced. Although the dipole–dipole interactions of two nuclei depend on values of the spectral density function at five frequencies (zero frequency, resonance frequencies of both nuclei, and their sum and difference), the large difference between magnetogyric ratios of ^{1}H and ^{15}N makes three high-frequency values of the spectral density function similar. In protein relaxation studies, it is common to replace the high-frequency spectral density values with a single effective value. Such an approach is known as *reduced spectral density mapping* (Ishima and Nagayama 1995a, b; Farrow et al. 1995) and simplifies the definitions of all relaxation rates to linear combinations of three (or less) spectral density values.

In principle, the outlined approach is applicable to both structured and unstructured proteins. However, attention should be paid to several issues when analyzing the ^{15}N relaxation rates of IDPs. First, the high-frequency values of spectral density function contribute more to the relaxation in IDPs than in well-ordered proteins. Therefore, the differences among the high-frequency values are more significant. Second, the higher signal-to-noise ratio of IDP spectra due to a narrower linewidth of signals allows us to obtain more precise data. Therefore, systematic errors that can be neglected in studies of well-folded proteins may became significant for IDPs. Third, the effects of small deviations of the symmetry axis of the ^{15}N chemical shift tensor from the direction of the ^{15}N–^{1}H bond are potentially suppressed by isotropic tumbling of well-ordered proteins. In the case of IDPs, the global rotational diffusion cannot be separated from internal motions. Therefore, anisotropy of the molecular motions is difficult to assess.

In this paper, reliability of the ^{15}N reduced spectral density mapping applied to IDPs is addressed. Various sources of systematic errors are analyzed for the traditional approach and for newly designed methods utilizing cross-correlated relaxation rates. Optimal protocols describing fast and slow dynamics are proposed and their practical applicability is documented for a partially disordered delta subunit of bacterial RNA polymerase.

Materials and methods

Sample preparation

The *rpoE* gene encoding the δ subunit of RNA polymerase from *Bacillus subtilis* (plasmid pFL31) was expressed in the *Escherichia coli* BL21(DE3) strain in 2 L of the M9 medium containing [^{15}N] ammonium chloride as a sole source of nitrogen. The obtained protein was purified as described earlier (DeSaro et al. 1995). A 0.8 mM δ subunit sample was prepared in 20 mM phosphate buffer, pH* 6.6 (uncorrected reading) containing 10 mM sodium chloride, 10 % deuterium oxide, and 0.05 % sodium azide.

NMR experiments

The measurements were performed at 500 and 600 MHz Bruker Avance III spectrometers equipped with room-temperature TXI and cryogenic TCI probeheads, respectively, at the temperature of 300.2 K. Temperature was calibrated according to the chemical shift differences of pure methanol peaks. Delays of the polarization transfer periods in protein backbone and nucleic acid bases were set for 90 Hz ^{15}N–^{1}H coupling. The program NMRPipe (Delaglio et al. 1995) was used to process the data. Data was processed with the cosine square apodization and four-fold zero filling. The phase in the direct dimension was manually adjusted to pure absorption. The spectra were analyzed and the peak heights were evaluated in the program Sparky 3.115 (T.D. Goddard and D. G. Kneller, University of California, San Francisco, USA). The resonances were assigned according to the literature (Motáčková et al. 2010a). Relaxation rates measured by varying relaxation delays were obtained by fitting peak intensities to a mono-exponential decay using programs Relax (d'Auvergne and Gooley 2008a, b) for R_1 and R_2 and Octave (J. Eaton, University of Wisconsin, Madison, USA) for other rates.

Values of R_1, R_2, and ^{15}N–^{1}H steady-state nuclear Overhauser effect (NOE) at the 600 MHz spectrometer were determined within a previous study (Papoušková et al. 2013) and deposited in the Biological Magnetic Resonance Data Bank (http://www.bmrb.wisc.edu) as entry 19284. Standard experiments (Korzhnev et al. 2001) were used for the measurements of R_1, with relaxation delays of 22.4, 67.2, 134.4*, 246.4, 380.8, 560*, 784, 1,008, and 1,232 ms, and of R_2, with relaxation delays of 0, 17.283, 34.566*, 51.850, 69.133, 86.416*, 103.699, 138.266, and 172.832 ms, at 500 MHz. The asterisk denotes the spectra recorded twice in order to estimate the

experimental error. The R_2 rates were measured with the delay between the 180° pulses in the CPMG train equal to 1.0 ms. The R_2 experiment at 600 MHz, previously performed with the CPMG delay of 0.9 ms (Papoušková et al. 2013), was repeated with CPMG delay of 1.4 ms and relaxation delays of 0, 23.546, 47.091*, 70.637, 94.182, 117.728*, 141.274, 188.365, and 235.456 ms. A relaxation compensated CPMG experiment (Long et al. 2008) with CPMG frequency ranging from 50 to 1,000 Hz was used to qualitatively verify the presence of a slow exchange. The ^{15}N–^{1}H steady-state nuclear Overhauser effect at 600 MHz (Ferrage et al. 2009) was measured with a 20 s inter-scan relaxation delay and 226 repeats of 180° ^{1}H pulses separated by 22.22 ms delay were used to achieve a steady state. The reference spectra were measured interleaved together with the spectra under the steady state conditions. The experimental error was evaluated based on three independent measurements. The transverse cross-correlated relaxation rates Γ_x were measured at 500 MHz using IPAP-HSQC (Hall et al. 2003; Hall and Fushman 2003) with relaxation delays of 11.1, 22.2, 44.4, 66.6*, 88.8, and 111.1 ms, where the asterisk denotes the spectra recorded three times. The in-phase and anti-phase spectra were combined in a ratio optimized for each residue to obtain a pure up-field and down-field component of the doublet. The value of Γ_x was obtained by fitting the ratio of heights of the up-field and down-field peaks to the mono-exponential decay. More accurate experiments based on symmetrical reconversion were used at 600 MHz for determination of transverse cross-correlated relaxation rate Γ_x (Pelupessy et al. 2003) and longitudinal cross-correlated relaxation rate Γ_z (Pelupessy et al. 2007) at 600 MHz. The transverse cross-correlated relaxation rates were determined from peak intensities in spectra recorded with 50 and 70 ms relaxation delays and the longitudinal cross-correlated relaxation rates from peak intensities in spectra recorded with 100, 175, and 250 ms relaxation delays.

Standard deviation of the peak intensities was estimated from the noise using Monte-Carlo simulations. The measured experimental data were deposited in the Biological Magnetic Resonance Data Bank (http://www.bmrb.wisc.edu) as entry 18903.

Analysis of relaxation rates

The semi-classical theory of spin relaxation in isotropic liquids (Wangsness and Bloch 1953; Redfield 1965) was applied in order to interpret the relaxation rates in terms of values of the spectral density function (Korzhnev et al. 2001). In order to simplify the analysis of relaxation rates formally, the measured auto-relaxation rates R_1 and R_2, heteronuclear Overhauser enhancement defined as a ratio of peak intensities in the steady-state (I_{ss}) and reference (I_{ref}) spectra, and cross-correlated relaxation rates Γ_x and Γ_z were rescaled to the same units as the spectral density values:

$$\delta = (2R_2 - R_1)/d^2, \tag{1}$$

$$\rho = R_1/d^2, \tag{2}$$

$$\sigma = \frac{\gamma_N}{\gamma_H}\left(\frac{I_{ss}}{I_{ref}} - 1\right)R_1/d^2, \tag{3}$$

$$\mu = b\Gamma_x/(pcd), \tag{4}$$

$$\lambda = b\Gamma_z/(pcd), \tag{5}$$

where $b = 1 + c^2/d^2, d = -\mu_0 h\gamma_H\gamma_N/(16\pi^2 r_{HN}^3\sqrt{5})$, $c = \gamma_N B_0\Delta_N/(3\sqrt{5})$, γ_H and γ_N are the magnetogyric ratios of ^{1}H and ^{15}N, respectively, r_{HN} is the ^{1}H–^{15}N internuclear distance, μ_0 is the permeability of vacuum, h is the Planck's constant, Δ_N is the anisotropy of the ^{15}N chemical shift tensor, $p = (3\cos^2\theta_{c,d} - 1)/2$, $\theta_{c,d}$ is the angle between the ^{1}H–^{15}N bond and the symmetry axis of the ^{15}N chemical shift tensor, and B_0 is the induction of the external magnetic field. Values of $r_{HN} = 0.102$ nm and $\Delta_N = -170$ ppm were used in this study (Tjandra et al. 1996). Value of $\theta_{c,d}$ was optimized to obtain equal values of auto- and cross-correlated spectral density functions at the ^{15}N frequency in the disordered region of the protein (see "Results and discussion" section). The obtained optimal $\theta_{c,d}$ was 22.5°.

The rescaled relaxation rates were assumed to be given by the following linear combinations of spectral density functions (Korzhnev et al. 2001):

$$\delta = 2\xi + 8b\overline{J}(0) + 12J^{dd}(\omega_H), \tag{6}$$

$$\rho = 6b\overline{J}(\omega_N) + 2J^{dd}(\omega_H - \omega_N) + 12J^{dd}(\omega_H + \omega_N), \tag{7}$$

$$\sigma = -2J^{dd}(\omega_H - \omega_N) + 12J^{dd}(\omega_H + \omega_N), \tag{8}$$

$$\mu = 2b(4J^{cd}(0) + 3J^{cd}(\omega_N))/p, \tag{9}$$

$$\lambda = 12bJ^{cd}(\omega_N)/p, \tag{10}$$

where $J^{dd}(\omega)$ and $J^{cc}(\omega)$ are the auto-correlation spectral density functions describing reorientation of the N–H bond and of the principle axes of the ^{15}N chemical shift tensor, respectively, $J^{cd}(\omega)$ is the cross-correlation spectral density functions describing interference between the ^{15}N chemical shift anisotropy and ^{1}H–^{15}N dipole–dipole interactions, $\xi = R_{ex}/d^2$ is the slow exchange contribution, and $\overline{J}(\omega) = (J^{dd}(\omega) + c^2J^{cc}(\omega)/d^2)/b$. Various methods of solving Eqs. 6–10 are discussed in "Results and discussion" section.

Results and discussion

Reduced spectral density mapping

In general, three spectral density functions $J^{dd}(\omega)$, $J^{cc}(\omega)$, and $J^{cd}(\omega)/p$, contributing to the relaxation rates described by Eqs. 6–10, differ. However, they can be replaced with a single function $J(\omega)$ if the molecule moves isotropically or, in case of motional anisotropy, if the symmetry axis of the ^{15}N chemical shift tensor is collinear with the N–H bond (Korzhnev et al. 2001). Equations 6–10 then represent a set of five linear combinations of five discrete values of the same spectral density function. All five $J(\omega_k)$ values can be calculated easily if all five relaxation rates are measured and if the exchange contribution ξ is negligible or determined separately. If a slow conformational exchange contributes to R_2, values of $J(0)$, $J(\omega_N)$, $J(\omega_H + \omega_N)$, and $J(\omega_H - \omega_N)$ can be calculated from R_1, NOE, Γ_x, and Γ_z (rescaled to ρ, σ, μ, and λ, respectively), using Eqs. 7–10. In practice, it is often impossible to follow such an ideal route. Some relaxation rates may be difficult to obtain with a sufficient precision and accuracy, or motional anisotropy combined with mutual orientation of individual interaction vectors does not permit to use a single spectral density function. In such cases, the number of $J(\omega_k)$ values is higher than the number of relaxation rates measured at each magnetic field. It is therefore necessary to reduce the number of $J(\omega_k)$ values in order to make their extraction from the limited set of the experimental data possible. The present study proposes and compares several reduction procedures. They are described by the types of relaxation rates used, abbreviated L for the longitudinal auto-relaxation rate R_1, T for the transverse auto-relaxation rate R_2, N for the heteronuclear steady-state NOE, X for the transverse cross-correlated relaxation rate Γ_x, and Z for the longitudinal cross-correlated relaxation rate Γ_z.

Analysis of R_1, R_2, and NOE: LTN

The original application of reduced spectral density mapping (Ishima and Nagayama 1995a, b; Farrow et al. 1995) is based on the assumption that $\omega_H \gg \omega_N$ at any magnetic field. The reduction of the number of $J(\omega_k)$ values is achieved by replacing $J^{dd}(\omega_H - \omega_N)$, $J^{dd}(\omega_H)$, and $J^{dd}(\omega_H + \omega_N)$ with a single value $J^{dd}(\varepsilon\omega_H)$. If three high-frequency spectral density values in Eqs. 6, 7, and 8 are substituted with a single effective one $J^{dd}(\varepsilon\omega_H)$, δ, ρ, and σ can be approximated by linear combinations of three spectral density values $\overline{J}(0)$, $\overline{J}(\omega_N)$, and $J^{dd}(\varepsilon\omega_H)$. These values can be calculated from Eqs. 6, 7, and 8.

Farrow et al. derived the value of ε which makes $J^{dd}(\varepsilon\omega_H)$ equal to $\sigma/10$ (cf. Eq. 8) if the spectral density function can be can be approximated as $\lambda_1/\omega^2 + \lambda_2$ (Farrow et al. 1995). Therefore, $J^{dd}(\varepsilon\omega_H)$ representing the effective high-frequency term in Eq. 8 can be obtained very accurately if it is calculated for the optimized value of ε. However, this value of $J^{dd}(\varepsilon\omega_H)$ differs from $J^{dd}(\omega_H)$ and from $(6J^{dd}(\omega_H + \omega_N) + J^{dd}(\omega_H - \omega_N))/7$, which represent the high-frequency terms in Eqs. 6 and 7, respectively. As a consequence, replacing the high-frequency terms in Eqs. 6 and 7 by the optimized $J^{dd}(\varepsilon\omega_H)$ value results in a systematic error, referred to as *reduction bias* in this paper. In the simplest version of the reduced spectral density mapping developed by Farrow et al. (Method 1), the deviations of the calculated zero- and low-frequency spectral density values from real $\overline{J}(0)$ and $\overline{J}(\omega_N)$, respectively, are neglected (Farrow et al. 1995). Such an approximation is likely to have only a negligible effect on the accuracy of calculated spectral density values in the case of well-folded proteins. However, the systematic errors become significant if sub-nanosecond motions dominate the dynamics. In such a case, the reduction bias may exceed 8 % of the spectral density values (see Fig. S1 in Supplementary Material). Therefore, Method 1 is not suitable for spectral density mapping of IDPs: the neglected differences among the high-frequency spectral density values, which become important for highly flexible residues of IDPs, are accounted for properly when calculating the effective high-frequency spectral density value, but not when estimating the zero- and low-spectral density density values. Among improved versions of the reduced spectral density mapping proposed by Farrow et al., we found Method 3 (Farrow et al. 1995) most suitable for IDPs, and applied it in our study.

Our optimized protocol, referred to as approach LTN, is based on approximating $J^{dd}(\omega)$ with a linear function between $J^{dd}(\omega_H + \omega_N)$ and $J^{dd}(\omega_H - \omega_N)$ with a slope $s = \Delta J^{dd}(\omega)/\Delta\omega$ calculated from NOE data acquired at two magnetic fields (Farrow et al. 1995). The linear approximation is equivalent to the assumption $\beta_+ = \beta_-$, where $\beta_+ = J^{dd}(\omega_H + \omega_N) - J^{dd}(\omega_H)$ and $\beta_- = J^{dd}(\omega_H) - J^{dd}(\omega_H - \omega_N)$. In such a case, the reduction bias can be suppressed by applying corrections proportional to $s\omega_N$ to the solution of Eqs. 6–8:

$$J^{LTN}(0) = \frac{5\delta - 6\sigma}{40b} + \frac{21s\omega_N}{10b}, \tag{11}$$

$$J^{LN}(\omega_N) = \frac{5\rho - 7\sigma}{30b} + \frac{8s\omega_N}{5b}, \tag{12}$$

$$J^{LN}(\varepsilon\omega_H) = \frac{\sigma}{10}, \tag{13}$$

where the superscripts refer to the relaxation rates used to calculate the given spectral density value. The coefficient ε in Eq. 13 is equal to 0.858, a value close to $\varepsilon = 0.870$

obtained by approximating the spectral density function as $\lambda_1/\omega^2 + \lambda_2$ (Farrow et al. 1995).

Spectral density values obtained as described by Eqs. 11–13 and by the protocols discussed below with the details of the calculation (uncorrected equations, corrections) and with various types of systematic errors, including the reduction bias, are listed in Table 1. Note that the linear approximation of the spectral density function is equivalent to the assumption $\beta_+ = \beta_- = s\omega_N$, when the corrections listed in Table 1 match the reduction bias exactly. Systematic errors of spectral density values calculated with and without the corrections were simulated for a model case of a single-Lorentzian spectral density function (see Fig. S1 in Supplementary Material). Fig. S1 documents efficiency of the corrections for various correlation times. The residual reduction bias did not exceed 3 % when the corrections were applied.

Table 1 also reviews propagation of random errors for individual calculated spectral density values. In reality, the final errors depend on the equations used to calculate the given value, on experimental errors of all relaxation rates employed in the calculation, and on the actual values of the spectral density function which determine the employed relaxation rates. In order to provide a simple comparison, relative errors of $R_1, R_2, \Gamma_x, \Gamma_z$, and of $(I_{ss}/I_{ref} - 1)$ were assumed to be identical and an error multiplication factor m was expressed as a ratio of the relative error of the calculated spectral density value to the relative error of the relaxation rates. Furthermore, the influence of the high-frequency contributions to the relaxation rates was described only in two limiting cases, (1) for motions sufficiently slow, when the high-frequency spectral density values are much lower than $\overline{J}(0)$ and $\overline{J}(\omega_N)$ and can be neglected, and (2) for very fast motions, when $J^{dd}(\omega_H + \omega_N) \approx J^{dd}(\omega_H) \approx J^{dd}(\omega_H - \omega_N) \approx \overline{J}(\omega_N) \approx \overline{J}(0)$. In the former case (sufficiently slow dynamics), $m \approx \sqrt{u^2 + v^2X + w^2X^2}$, where $X = 3\overline{J}(\omega_N)/(4\overline{J}(0))$ and the coefficients u, v, w are listed in Table 1. In the latter case (limit of very fast dynamics), $X = 3/4$ and $m \approx \sqrt{u^2 + 3v^2/4 + 9w^2/16 + f^2}$, where f represents the high frequency contributions.

The values of u, v, w, and f listed in Table 1 give the multiplication factor of $J^{LTN}(0)$ and $J^{LN}(\omega_N)$ equal to 4.9 and 3.6, respectively, for very fast motions. Relaxation rates of residues with fast dynamics are measured with low experimental errors (errors determined from the signal-to-

Table 1 List of apparent values of the spectral density function calculated using different approaches described in this paper and of their errors

$J(\omega)$	Source	Approach	Uncorrected equation	Correction	Bias			Error propagation	
					Reduction[a]	Exch.	Orient.	u, v, w	f
$\overline{J}(0)$	R_1, R_2, NOE	LTN	$J^{LTN}(0) = \frac{5\delta-6\sigma}{40b}$	$+\frac{21s\omega_N}{10b}$	$-\frac{18\beta_+ + 3\beta_-}{10b}$	$+\frac{\xi}{4b}$	0	1.00, 1.41, 1.41	4.48
$\overline{J}(0)$	Γ_x, Γ_z	XZ	$J^{XZ}(0) = \frac{2\mu-\lambda}{16b}$	0	0	0	$-\frac{\alpha_0}{4b}$	1.00, 1.41, 1.41	0
$\overline{J}(0)$	R_1, NOE, Γ_x	LNX	$J^{LNX}(0) = \frac{5\mu-5\rho+7\sigma}{40b}$	$-\frac{6s\omega_N}{5b}$	$+\frac{3\beta_+ + 3\beta_-}{5b}$	0	$-\frac{\alpha}{4b}$	1.00, 1.41, 1.41	2.62
$\overline{J}(0)$	R_1, R_2, Γ_x	LTX	$J^{LTX}(0) = \frac{7\delta-6\rho+6\mu}{104b}$	$+\frac{15s\omega_N}{26b}$	$-\frac{18\beta_+ - 3\beta_-}{26b}$	$+\frac{7\xi}{52b}$	$-\frac{3\alpha}{26b}$	0.71, 1.00, 1.00	2.43
$J^{cd}(0)$	Γ_x, Γ_z	XZ	$J^{cd}(0) = \frac{2\mu-\lambda}{16b}p$	0	0	0	0	1.00, 1.41, 1.41	0
$\overline{J}(\omega_N)$	R_1, NOE	LTN, LNX	$J^{LN}(\omega_N) = \frac{5\rho-7\sigma}{30b}$	$+\frac{8s\omega_N}{5b}$	$-\frac{4\beta_+ + 4\beta_-}{5b}$	0	0	1.00, 0.00, 0.00	3.50
$\overline{J}(\omega_N)$	Γ_z	XZ	$J^{Z}(\omega_N) = \frac{\lambda}{12b}$	0	0	0	$-\frac{\alpha_N}{3b}$	1.00, 0.00, 0.00	0
$\overline{J}(\omega_N)$	R_1, R_2, Γ_x	LTX	$J^{LTX}(\omega_N) = \frac{6\rho-7\delta+7\mu}{78b}$	$-\frac{10s\omega_N}{13b}$	$+\frac{12\beta_+ - 2\beta_-}{13b}$	$-\frac{7\xi}{39b}$	$-\frac{7\alpha}{39b}$	$\frac{0.76}{X}, \frac{1.08}{X}, \frac{1.04}{X}$	3.23
$J^{cd}(\omega_N)$	Γ_z	XZ	$J^{cd}(\omega_N) = \frac{\lambda}{12b}p$	0	0	0	0	1.00, 0.00, 0.00	0
$J^{dd}(\varepsilon\omega_H)$	R_1, NOE	LTN, LNX	$J^{LN}(\epsilon\omega_H) = \frac{\sigma}{10}$	0	(0)[b]	0	0	1.41, 0.00, 0.00	(0)[b]
$J^{dd}(\varepsilon\omega_H)$	R_1, R_2, Γ_x	LTX	$J^{LTX}(\varepsilon\omega_H) = \frac{\rho+\delta-\mu}{26}$	0	(0)[b]	$+\frac{\xi}{13}$	$+\frac{\alpha}{13}$	$\frac{1.41}{Y}, \frac{2.00}{Y}, \frac{2.00}{Y}$	1.93

The reduction bias is expressed in terms of $\beta_+ = J^{dd}(\omega_H + \omega_N) - J^{dd}(\omega_H)$ and $\beta_- = J^{dd}(\omega_H) - J^{dd}(\omega_H - \omega_N)$. The exchange bias is described by $\xi = R_{ex}/d^2$. Parameters α_0, α_N, and α, describing the orientational bias, are defined as $\alpha_0 = 4b(\overline{J}(0) - J^{cd}(0)/p)$, $\alpha_N = 3b(\overline{J}(\omega_N) - J^{cd}(\omega_N)/p)$, and $\alpha = \alpha_0 + \alpha_N$. Propagation of the experimental error was calculated according to the variance formula (neglecting correlation of variables and assuming $\xi = 0$, $\alpha = 0$), and is described by parameters u, v, w, and by the contribution of the high-frequency terms in the limit of fast motions, f. The error multiplication factor m for identical relative errors of $R_1, R_2, \Gamma_x, \Gamma_z$, and of $(I_{ss}/I_{ref} - 1)$ is given by $m = \sqrt{u^2 + 3v^2/4 + 9w^2/16 + f^2}$ for very fast motions and by $\sqrt{u^2 + v^2X + w^2X^2}$, where $X = 3\overline{J}(\omega_N)/(4\overline{J}(0))$, for motions slow enough to neglect the high-frequency contributions. The values of f are listed for data acquired at a 600 MHz spectrometer. The dependence of the random error of $J^{LTX}(\varepsilon\omega_H)$ on relaxation rates including $J(0)$ contributions is described by the parameter $Y = 13J^{dd}(\varepsilon\omega_H)/(4b\overline{J}(0))$

[a] If no correction is applied

[b] If ε is optimized so that $6J^{dd}(\omega_H + \omega_N) - J^{dd}(\omega_H - \omega_N) = 5J^{dd}(\varepsilon\omega_H)$ for LTN and LNX, and $6J^{dd}(\omega_H + \omega_N) + 6J^{dd}(\omega_H) + J^{dd}(\omega_H - \omega_N) = 13J^{dd}(\varepsilon\omega_H)$ for LTX

noise ratio in this study were lower than 1 % for the disordered domain of the studied protein). Therefore, the fivefold increase of the relative error is well acceptable for IPDs. The error multiplication factor drops down when slower motions dominate and contributions of high-frequency terms vanish. For negligible high-frequency contributions, the relative error of $J^{\mathrm{LN}}(\omega_{\mathrm{N}})$ is equal to the relative error of R_1. Propagation of the error of $J^{\mathrm{LTN}}(0)$ depends on both zero- and low-frequency contributions of the spectral density function to the relaxation rates. Although the spectral density values of IDPs are far from the limit of slow motions ($X = 0$, with the multiplication factor equal to $u = 1$), the values of X observed in this study ($X < 0.4$ for residues with $J^{\mathrm{LTN}}(0) > 1$ ns/rad, vide infra) predict the relative error of the determined $J^{\mathrm{LTN}}(0)$ value only slightly higher than the relative experimental error of relaxation rates ($m < 1.5$ for $J^{\mathrm{LTN}}(0) > 1$ ns/rad).

It should be emphasized that the simplified error propagation analysis, described above, served only for a general comparison of precision of various protocols presented in this paper. The actual errors of spectral density values calculated from experimental data were treated more rigorously using complete covariance matrices (vide infra).

Exchange-free mapping: XZ, LNX, LNXT

The transverse auto-relaxation rate, R_2 is potentially affected by a slow chemical or conformational exchange (Korzhnev et al. 2001). This fact makes R_2 a useful source of information on slow molecular motions and processes, but it also complicates calculation of the spectral density values, as the exchange contribution introduces an additional systematic error (*exchange bias*). It follows from Eq. 6 that the exchange increases the calculated $J^{\mathrm{LTN}}(0)$ value by a factor of $\xi/4b$ (Table 1). In order to separate the exchange contribution from the $J(\omega_k)$ terms, ξ must be determined independently or a different spectral density protocol must be applied.

The trivial solution is to avoid analysis of R_2 and to calculate only $J^{\mathrm{LN}}(\omega_{\mathrm{N}})$ and $J^{\mathrm{LN}}(\varepsilon\omega_{\mathrm{H}})$ from Eqs. 12 and 13, respectively. However, an exchange-free zero-frequency spectral density value can be also obtained if the cross-correlated relaxation rates are employed.

One possibility is to acquire and analyze cross-correlated relaxation rates only. The cross-correlated relaxation rates Γ_x and Γ_z are easiest to analyze but most difficult to measure (Hall et al. 2003; Hall and Fushman. 2003; Pelupessy et al. 2007). If favorable relaxation properties of IDPs counterbalance the inherently low sensitivity of the Γ_x and Γ_z measurement, the spectral density values $J^{\mathrm{cd}}(0)/p$ and $J^{\mathrm{cd}}(\omega_{\mathrm{N}})/p$ are calculated exactly from Eqs. 9 and 10 without a need of any reduction (protocol XZ):

$$J^{\mathrm{XZ}}(0) = J^{\mathrm{cd}}(0)/p = (2\mu - \lambda)/16b, \tag{14}$$

$$J^{\mathrm{Z}}(\omega_{\mathrm{N}}) = J^{\mathrm{cd}}(\omega_{\mathrm{N}})/p = \lambda/12b. \tag{15}$$

By definition, the $J^{\mathrm{cd}}(0)$ and $J^{\mathrm{cd}}(\omega_{\mathrm{N}})$ values are not influenced by the reduction or exchange bias. As such, they may serve as an ideal reference for $\overline{J}(0)$ and $\overline{J}(\omega_{\mathrm{N}})$, respectively. Such comparison relies on correct ratios of the constants c, d, and p, i.e., on using accurate values of r_{HN}, Δ_{N}, and $\theta_{\mathrm{c,d}}$.

Another approach is to combine auto- and cross-correlated relaxation rates. As mentioned above, determination of exchange-free $J^{\mathrm{LN}}(\omega_{\mathrm{N}})$ and $J^{\mathrm{LN}}(\varepsilon\omega_{\mathrm{H}})$ from R_1 and NOE according to Eqs. 12 and 13, respectively, is straightforward and explicit. Therefore, combination of auto- and cross-correlated relaxation rates is needed only to obtain exchange-free $J(0)$. The exchange bias is avoided if $J(0)$ is calculated from a set of R_1, NOE, and Γ_x, none of which is influenced by the slow exchange (the LNX approach). This approach has the advantage that three spectral density values are obtained and the most difficult Γ_z measurement can be avoided. However, combination of auto- and cross-correlated relaxation rates also presents a certain challenge. The exact solution of Eqs. 7–9 requires that $J^{\mathrm{cd}}(\omega) = p\overline{J}(\omega)$. This condition is fulfilled if all motions contributing to the relaxation are isotropic or, in case of motional anisotropy, if the chemical shielding tensor is axially symmetric and its symmetry axis is collinear with the direction of the N–H bond. Otherwise, $\overline{J}(0)$ is calculated with a systematic error, referred to as *orientational bias* in this study.

Evaluation of $\overline{J}(0)$ from R_1, NOE, and Γ_x can be described as

$$J^{\mathrm{LNX}}(0) = \frac{5\mu - 5\rho + 7\sigma}{40b} - \frac{6s\omega_{\mathrm{N}}}{5b}. \tag{16}$$

Fig. S1 in Supplementary Material shows that the reduction bias of $J^{\mathrm{LNX}}(0)$ is lower than that of $J^{\mathrm{LTN}}(0)$. Neglecting the reduction bias, $\overline{J}(0)$ differs from $J^{\mathrm{LNX}}(0)$ by a factor of $\alpha/4b$ (Table 1), where $\alpha = \alpha_0 + \alpha_{\mathrm{N}}$ represents (an unknown) orientational bias, defined as

$$\alpha_0 = 4b(\overline{J}(0) - J^{\mathrm{cd}}(0)/p) \tag{17}$$

and

$$\alpha_{\mathrm{N}} = 3b(\overline{J}(\omega_{\mathrm{N}}) - J^{\mathrm{cd}}(\omega_{\mathrm{N}})/p). \tag{18}$$

If the analysis is extended to R_2 (approach LNXT), $\xi + \alpha$ can be evaluated as

$$\xi + \alpha = \frac{5\rho + 5\delta - 5\mu - 13\sigma}{10} + \frac{66s\omega_{\mathrm{N}}}{5}, \tag{19}$$

but the contributions of ξ and α cannot be distinguished. The reduction bias of the obtained exchange contribution

simulated for a Lorentzian spectral density function is negligible (Fig. S1d in Supplementary Material).

The error propagation is identical for the LTN, XZ, and LNX protocols when the high-frequency contributions are negligible (see values of u, v, w in Table 1). Relative errors in the limit of fast motions are lower for both XZ and LNX protocols than those of the LTN analysis (see values of f in Table 1).

Combination of R_1, R_2, and Γ_x: LTX

The transverse cross-correlated relaxation rate Γ_x can be also combined with auto-relaxation rates R_1 and R_2 (LTX approach). The spectral density values can be then calculated from δ, ρ, and μ by combining Eqs. 6, 7, and 9. If NOE data at two magnetic fields are also available, the reduction bias can be corrected in a similar manner as discussed for the LTN approach.

$$J^{\mathrm{LTX}}(0) = \frac{7\delta - 6\rho + 6\mu}{104b} + \frac{15s\omega_{\mathrm{N}}}{26b}, \tag{20}$$

$$J^{\mathrm{LTX}}(\omega_{\mathrm{N}}) = \frac{6\rho - 7\delta + 7\mu}{78b} - \frac{10s\omega_{\mathrm{N}}}{13b}, \tag{21}$$

$$J^{\mathrm{LTX}}(\varepsilon\omega_{\mathrm{H}}) = \frac{\rho + \delta - \mu}{26}. \tag{22}$$

In principle, Eqs. 20–22 provide values of the spectral density function at zero, low and high frequency. In practice, propagation of random errors makes LTX less favorable (see Table 1). The reason is that calculation of small values of $J^{\mathrm{LTX}}(\omega_{\mathrm{N}})$ and $J^{\mathrm{LTX}}(\varepsilon\omega_{\mathrm{H}})$ includes a subtraction of two relatively large terms, δ and μ. As a consequence, parameters u, v, and w are divided by X or Y, defined in Table 1. The error multiplication factor rapidly grows for slow motions, as the ratios X and especially Y decrease with increasing correlation times (due to increasing $\overline{J}(0)$ and decreasing low- and high-frequency values). In case of IDPs, relaxation rates can be measured with a precision sufficient for a reliable determination of $J^{\mathrm{LTX}}(\omega_{\mathrm{N}})$. The error multiplication is less than five-fold for $J^{\mathrm{LTX}}(\omega_{\mathrm{N}})$ of disordered residues analyzed in this study (vide infra). However, the error propagation analysis shows that sufficiently precise determination of $J^{\mathrm{LTX}}(\varepsilon\omega_{\mathrm{H}})$ would require unrealistically low experimental errors of R_1, R_2, and Γ_x.

Systematic errors of the calculated spectral density values are also listed in Table 1. Compared to LNT and LNX, LTX has lower reduction bias (green curves in Fig. S1 in Supplementary Material) because Γ_x is independent of the high-frequency spectral density values. Similarly to LNX, the LTX protocol is most accurate when isotropic motions or axial symmetry and orientation of the shielding tensor reduce the orientational bias described by α. Finally, Table 1 shows that the LTX protocol is most affected by the exchange contribution.

In general, LTX cannot be recommended as an alternative of the LNT and LNX protocols. Note that Eqs. 20–22 are linear combinations of equations used in the LTN and LNX protocols. Therefore, LTX does not provide any new information if R_1, R_2, Γ_x, and NOE data are available and the LTN and LNX analyses have been carried out. Yet, the LTX approach can be useful in the following cases.

The LTX protocol can be applied when the NOE values are not available. In such a case, the reduction bias of the LTX protocol cannot be suppressed by applying the $s\omega_{\mathrm{N}}$ correction terms. In principle, Eqs. 6, 7, and 9 can be employed to calculate the slope of $J^{\mathrm{dd}}(\omega)$ in the same manner as used for calculating the slope from Eq. 8 in the case of approaches LTN or LNX. However, the large $\xi + \alpha$ contribution (compared to typical $J^{\mathrm{dd}}(\omega_k)$ values) makes this approach highly inaccurate in the presence of slow exchange or anisotropic motions. Since the reduction bias of the LTX protocol is low (vide supra), the optimal approach is to omit corrections in Eqs. 20 and 21 when analyzing R_1, R_2, and Γ_x only.

Another potential application of LTX is a quick and sensitive identification of slow exchange. LTX provides a better evidence of the slow exchange than LTN. As the exchange term appears only in Eq. 11, LTN overestimates $\overline{J}(0)$ by a factor of $\xi/4b$ if the exchange contribution is neglected. The other spectral density values remain unaffected. This can mask the effect of a fast internal motion that always lowers the value of $\overline{J}(0)$ (Lefèvre et al. 1996). On the contrary, the slow exchange contributes to $J^{\mathrm{LTX}}(\omega_{\mathrm{N}})$ even more than to $J^{\mathrm{LTX}}(0)$ in LTX (Eqs. 20 and 21). Since the $J^{\mathrm{LTX}}(\omega_{\mathrm{N}})$ values are smaller than $J^{\mathrm{LTX}}(0)$, the exchange contribution is more pronounced and less likely to be confused with a fast internal dynamics.

Case study: δ subunit of RNA polymerase

The goal of the case study was to test performance of the spectral density mapping protocols applied to ^{15}N relaxation data of a (partially) intrinsically disordered protein. The selected protein molecule, δ subunit of RNA polymerase from *Bacillus subtilis* (Pero et al. 1975; DeSaro et al. 1995; Rabatinová et al. 2013), consists of two distinct regions of similar size, N-terminal domain forming a well-defined structure and a long disordered C-terminal tail. This composition makes the δ subunit a good model system that allowed us to study relaxation of well-structured and intrinsically disordered protein residues within one molecule. Results of detailed investigation of the δ subunit, performed recently in our laboratory, provided us the necessary background for the relaxation analysis in a structural context. Structure of the well-folded N-terminal domain has been determined using NMR (Motáčková et al.

2010b). Assignment of the disordered and highly repetitive C-terminal tail (Motáčková et al. 2010a; Papoušková et al. 2013) made residue-specific relaxation studies of this region possible. Various experiments, including preliminary ^{15}N relaxation measurements, were applied to characterize behavior of the C-terminal domain (Papoušková et al. 2013).

The ^{15}N auto-relaxation rates R_1, R_2, cross-correlated relaxation rates Γ_x, Γ_z, and steady-state ^{15}N–^{1}H NOE were measured at two magnetic fields, corresponding to 500 and 600 MHz proton frequencies. The obtained spectral density values are presented in Fig. 1, where the calculated $\overline{J}(\omega_k)$ values are plotted as a function of calculated $\overline{J}(0)$. Such plots, referred to as *Lefèvre's plot* in this article, were

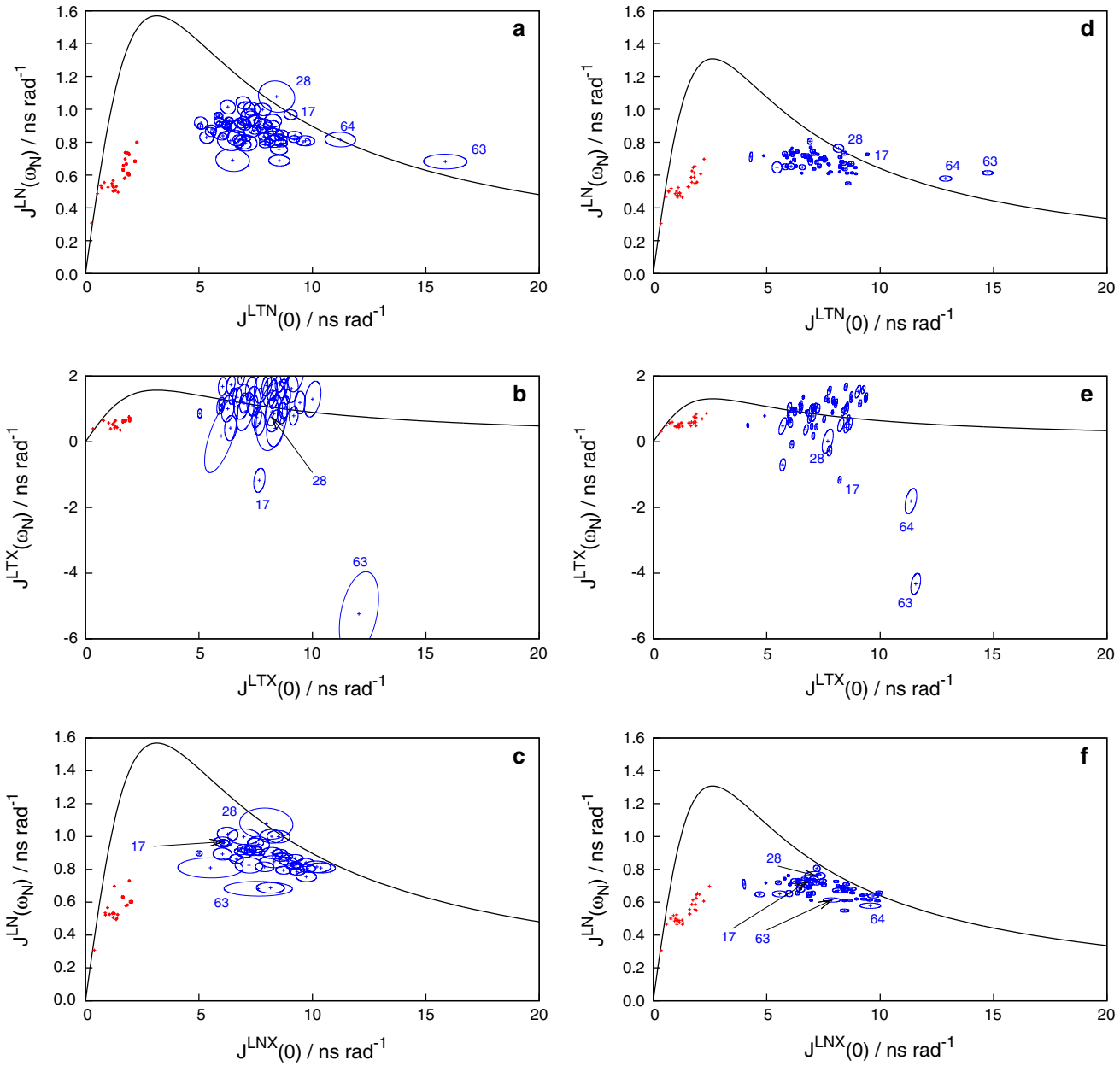

Fig. 1 Experimental $J(\omega_k)$ values obtained by LTN **(a, d)**, LTX **(b,e)**, and LNX **(c, f)**, applied to the relaxation data of the δ-subunit of RNA polymerase from *Bacillus subtilis*, measured at the 500 MHz **(a, b, c)** and 600 MHz **(d, e, f)** spectrometers. Data for residues from the well-structured N-terminal domain and disordered C-terminal region are displayed in *blue* and *red*, respectively. The errors of the obtained values were calculated by Monte-Carlo simulations from experimental errors of the relaxation rates used, and displayed as ellipses corresponding to two-dimensional projections of ellipsoids with the directions and squared relative lengths of the principal axes given by the eigenvectors and eigenvalues of the covariance matrix. Data for N–H bonds exhibiting the highest conformational exchange are labeled with residue numbers

proposed earlier as a graphical output of spectral density mapping allowing a straightforward interpretation (Lefèvre et al. 1996; Barthe et al. 1999; Křížová et al. 2004). If the spectral density values are expanded into a series of Lorentzian functions, the experimental point of each residue can be viewed as a weighted average of points along the solid curve in Fig. 1. For example, description of a residue in an isotropically tumbling molecule with internal dynamics fully determined by a single motional mode completely separated from overall rotational diffusion would require only two Lorentzian terms. In such a case, the actual spectral density value is represented by point R at the dotted line connecting points P and Q of the solid curve in Fig. 2, defined by the correlation time of the overall rotational diffusion, τ_0, (point P) and by the effective correlation time $\tau_1 = (\tau_i^{-1} + \tau_0^{-1})^{-1}$, where τ_i is the correlation time of the internal motion (point Q). The ratio of distances $|QR|/|PQ|$ is then equivalent to the generalized order parameter of the model-free approach (Lipari and Szabo 1982a, b; Halle et al. 1981). Although the experimental values, plotted in Fig. 1, cannot be in general decomposed into the individual contributions as shown in Fig. 2, they indicate what time scale of motions dominates dynamics of a given residue.

The $J(\omega_k)$ values of residues from the ordered and disordered domain are clearly separated into two clusters, distinguished by colors in Fig. 1. The blue cluster at high $J(0)$ reflects a major contribution of the overall rotational diffusion to the motions of the well-ordered N-terminal domain, while the red cluster at low $J(0)$ indicates that the dynamics of the disordered C-terminal region is much faster and independent of the overall tumbling. The plot also documents that very precise values were obtained for

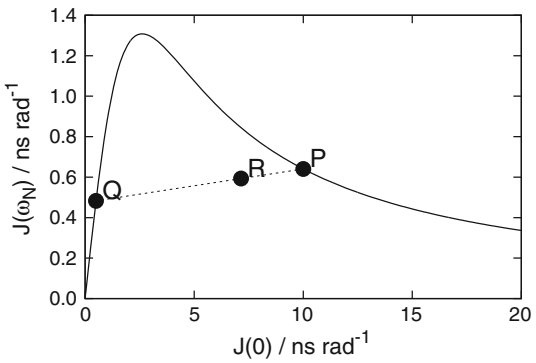

Fig. 2 Example of the Lefèvre's plot for $J(\omega_N)$ at the 600 MHz spectrometer. Points *P* and *Q* represent motional modes of a hypothetical residue whose dynamics is completely described by a spectral density function $J(\omega) = a_0 \ \tau_0/(1 + (\omega\tau_0)^2) + a_1 \ \tau_1/(1 + (\omega\tau_1)^2)$ with the correlation times $\tau_0 = 10$ ns and $\tau_1 = 0.5$ ns, respectively. Point *R* represents the resulting $J(0)$, $J(\omega_N)$ values calculated for contributions of the slow and fast motional modes equal to $a_0 = 0.7$ and $a_1 = 0.3$, respectively

residues in the disordered region (shown in red), in contrast to a relatively large error of values calculated for the well ordered N-terminal domain (blue), especially in the case of data acquired at 500 MHz using the room-temperature probehead.

When interpreting the obtained spectral density values, we first focused on residues of the N-terminal domain, representing the routinely studied case of a well-folded protein. As shown by simulations (Fig. S1 in Supplementary Material), the ^{15}N reduction bias is small for correlation times longer than 1 ns. Also, the orientational bias, described by the parameter α, is small for backbone amide ^{15}N, as its chemical shielding tensor is almost axially symmetric, with the symmetry axis close to the direction of the N–H bond (Yao et al. 2010). Therefore, all discussed methods are sufficiently accurate to analyze relaxation rates of amides from the structured part of the molecule, dominated by the overall tumbling. The only significant source of a bias of the calculated spectral density values is the contribution of the slow exchange. A visual inspection of the LTN plots (Fig. 1a) revealed four residues (V 17, K 28, N 63, and I 64) significantly influenced by a slow exchange. Interestingly, the LTX data (Fig. 1b), which is much more sensitive to the exchange, exhibited clear contributions of a slow exchange for most residues of the N-terminal domain. An independent CPMG relaxation dispersion experiment (Long et al. 2008) also indicated the slow exchange for additional residues, but the sensitivity did not allow a quantitative comparison (data not shown). Finally, the LNX data served as a source of spectral density values free of any exchange effect and allowed us to evaluate the exchange contributions to both LTN and LTX data. Without this comparison, the $J^{LTN}(0)$ values elevated by the exchange contribution in the LTN analysis could be misinterpreted as a higher rigidity of the corresponding residues. It documents that extending the standard analysis of R_1, R_2, and NOE to the cross-correlated relaxation rate Γ_x improves reliability of the reduced spectral density mapping, as it allows to clearly distinguish effects of slow motions from the fast dynamics.

After analyzing relaxation data of the N-terminal domain, we turned our attention to the disordered C-terminal region of the δ subunit. As mentioned in Introduction, there are several reasons why the relaxation data of disordered residues should be analyzed more carefully. First, in contrast to the rigid amino acids with dynamics dominated by a relatively slow overall tumbling, relaxation of flexible residues is much more influenced by motions with shorter correlation times. As a consequence, the reduction bias is higher (Fig. S1 in Supplementary Material). Second, it is difficult to estimate what systematic error is introduced by neglecting the difference between

$\overline{J}(\omega)$ and $J^{cd}(\omega)/p$ because motions of flexible residues cannot be described in terms of elements of the overall rotational diffusion tensor and its orientation with respect to the individual amide groups. Finally, the higher sensitivity, generally achieved for disordered residues, allows us to evaluate small differences of spectral density values with a good precision, but systematic errors safely neglected in the analysis of ordered proteins may become significant.

The relatively large difference between ^{1}H and ^{15}N resonance frequencies permits to greatly suppress the reduction bias by calculating correction factors from NOEs measured at two magnetic fields and applying them during the LTN and LNX analysis (Table 1, Fig. S1 in Supplementary Material).

The orientational bias represents a more serious problem, that complicates estimation of the exchange contribution by comparing outputs of individual protocols.

We decided to explore the orientational bias by (1) simulating the effect of α in a model case, (2) estimating α_N from the the difference between $J^{LN}(\omega_N)$ and $J^{Z}(\omega_N)$, available at 600 MHz, and (3) estimating α_0 from the zero-frequency spectral density values provided by different protocols.

In order to assess the effect of α theoretically, its values were first calculated for anisotropic motions simulated by an axially symmetric rotational diffusion tensor with $D_{\|}/D_{\perp} = 2$ for correlation times up to 3 ns. The values of α calculated for the most sensitive orientations varied between -0.93 ns/rad and $+1.23$ ns/rad for the 500 MHz spectrometer and between -0.89 ns/rad and $+1.15$ ns/rad for the 600 MHz spectrometer.

After gaining the first insight from the simulations, the real data was inspected. First, the spectral density values at ω_N, insensitive to the slow exchange, were examined. The favorable relaxation properties of the disordered C-terminal domain and a higher sensitivity of the 600 MHz spectrometer equipped with the cryogenic probehead allowed us to obtain relatively precise $J^{Z}(\omega_N)$ from the otherwise insensitive Γ_z measurements. In principle, the $J^{Z}(\omega_N)$ value, directly proportional to Γ_z, differs from $J^{LN}(\omega_N)$, calculated from R_1 and NOE, only by the factor $\alpha_N/3b$, describing the contribution to the orientational bias at the ^{15}N frequency (Eq. 18). In practice, the direct comparison also depends on the angle between the ^{15}N–^{1}H bond direction and the main axis of the ^{15}N chemical shift tensor, $\theta_{c,d}$. Since the $\theta_{c,d}$ values reported in the literature vary substantially, most likely as a consequence of a real variability of the chemical shift tensor in proteins (Yao et al. 2010), $\theta_{c,d}$ was optimized to achieve the same averages of $J^{Z}(\omega_N)$ and $J^{LN}(\omega_N)$ values in the disordered region. The optimal value of $\theta_{c,d}$ was 22.5° for the ^{15}N chemical shift anisotropy $\Delta_N = -170$ ppm. The choice of $\Delta_N = -160$ ppm would result in optimal $\theta_{c,d}$ of 21° and both $J^{LN}(\omega_N)$ and $J^{Z}(\omega_N)$ higher by 3 % (data not shown). The observed range of the $J^{LN}(\omega_N) - J^{Z}(\omega_N)$ differences indicates that α_N varies within ± 20 ps/rad in the C-terminal domain regardless of the choice of Δ_N, with an interesting exception of residues E 90–T 94, located close to the well-ordered N-terminal domain (Fig. 3a). This deviation might reflect differences in the shielding tensor due to a different conformational behavior of the mentioned proline-containing sequence ETQPT (Yao et al. 2010). The variations observed for the remaining residues of the C-terminal domain corresponded to 10 % of the range of the $J^{LN}(\omega_N)$ values calculated for the disordered region of the studied protein and to 3 % of the total $J^{LN}(\omega_N)$ range.

Estimation of the range of the zero-frequency contribution to the orientational bias, α_0, (Eq. 17) from the $J^{LTN}(0) - J^{XZ}(0)$ differences is less straightforward

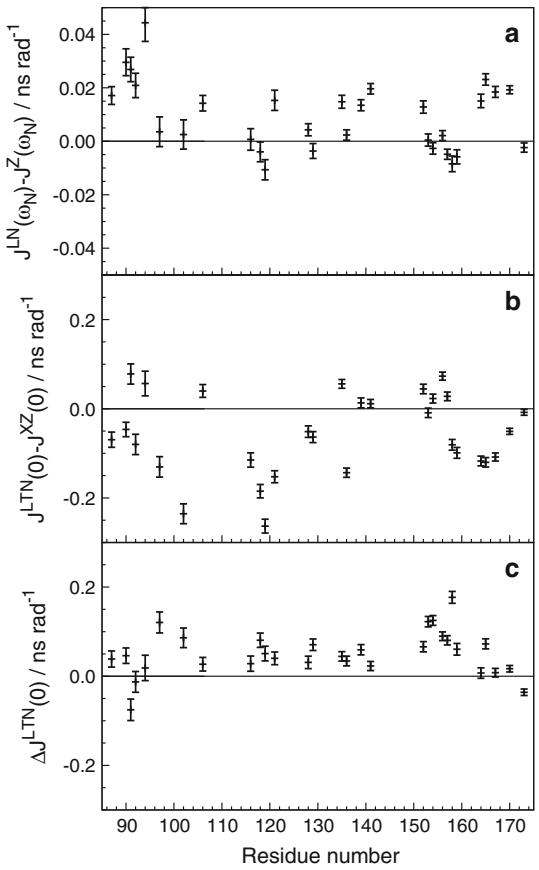

Fig. 3 Differences between the spectral density values obtained by LTN and XZ protocols at ω_N **(a)** and zero **(b)** frequencies, and the difference between $J^{LTN}(0)$ values calculated from R_2 measured with the delay of 1.4 and 0.9 ms between the pulses in the CPMG train **(c)**. The plotted values were calculated from data acquired at the 600 MHz spectrometer

because $J^{\mathrm{LTN}}(0)$ depends also on the slow exchange. The exchange contribution is suppressed in the R_2 experiment by applying the CPMG pulse train during the relaxation delay. However, the efficiency of the suppression is constrained by technical limits. In general, it is impossible to separate the ξ and α_0 contributions from the sum $\xi + \alpha_0$. Nevertheless, the physically allowed ranges of ξ and α_0 differ. While $\xi \geq 0$, α_0 can be positive or negative. As a consequence, lower $J^{\mathrm{LTN}}(0)$ than $J^{\mathrm{XZ}}(0)$ always indicates an α_0 contribution.

The $J^{\mathrm{LTN}}(0) - J^{\mathrm{XZ}}(0)$ differences in the C-terminal domain varied in a range of $\pm$ 0.2 ns/rad (Fig. 3b). This variation represents 15 % of the $J^{\mathrm{LTN}}(0)$ range of the disordered domain and 4 % of the $J^{\mathrm{LTN}}(0)$ range of the whole protein. Moreover, the $J^{\mathrm{LTN}}(0)$ values were not systematically higher than $J^{\mathrm{XZ}}(0)$. It indicates that the exchange effects were effectively suppressed by the CPMG train during the R_2 measurement because significant exchange contributions would result in a systematic positive deviation in Fig. 3b. If the ξ contributions are neglected, deviations in Fig. 3b correspond to α_0 within $\pm$ 0.2 ns/rad.

It should be emphasized that the analysis presented above provides only the upper limits of the orientational bias. The variations of values presented in Fig. 3a,b might be attributed to the orientational bias, experimental error, or varying $\theta_{\mathrm{c,d}}$ and/or Δ_{N} (Yao et al. 2010).

Values of $J^{\mathrm{LTN}}(0)$ and $J^{\mathrm{LN}}(\omega_{\mathrm{N}})$ higher by 3 % were obtained when using $\Delta_{\mathrm{N}} = -160$ ppm and $\theta_{c,d} = 21^{\circ}$ (data not shown). It documents that the choice of Δ_{N}, which depends on the local conformation (Yao et al. 2010), does not have a significant effect on the interpretation of the obtained values.

After estimating the possible systematic errors due to the orientational bias, we turned our attention to the interpretation of the spectral density values calculated for the disordered C-terminal domain of the δ subunit.

The experimental spectral density values calculated by applying the LTN, LNX, and XZ protocols are presented in Fig. 4a–c, respectively. The high-frequency $J^{\mathrm{dd}}(\varepsilon\omega_{\mathrm{H}})$ value, determined with a sufficient precision for the disordered residues, is plotted in Fig. 4d. Plots in Fig. 4a–c clearly show that the systematic errors discussed above are marginal and do not disturb the general agreement of the Lefèvre's plots obtained by different protocols (note that values plotted in Fig. 4a, c were calculated from data obtained in completely independent experiments). The auto-correlated values, plotted in Fig. 4a, are calculated from the relaxation data measured most routinely (R_1, R_2, and NOE), but are potentially influenced by a slow exchange (via R_2). The cross-correlated values, plotted in Fig. 4c, require running of much less sensitive experiments but are not influenced by any bias (including exchange effects). As a consequence, the correction based on data acquired at a different magnetic field is not needed. Therefore, spectral density values could be obtained also for residues whose peaks were not resolved at the lower field. Figure 4b represents a compromise, employing only the transverse cross-correlated relaxation rates that are easier to measure. The plotted values are not offset by the exchange but are potentially influenced by the orientational bias due to combining auto- and cross-correlated data. The high-frequency $J^{\mathrm{dd}}(\varepsilon\omega_{\mathrm{H}})$ values (Fig. 4d) are useful because they are far from the linear region of the Lefèvre's plot even for highly flexible residues. Therefore, they help to discriminate contributions of slower motions. A complete comparison of spectral density values calculated using different approaches is presented in Supplementary Material (Fig. S2). As discussed above, values obtained by the LTN, XZ, and LNX protocols are consistent, which validates the mentioned approaches. Higher deviations of the $J^{\mathrm{LTX}}(\omega_{\mathrm{N}})$ and $J^{\mathrm{LTX}}(\varepsilon\omega_{\mathrm{H}})$ values reflect higher errors for the LTX approach, in agreement with the theory (see Table 1).

The obtained picture of molecular motions of the C-terminal domain of the δ subunit is in a good agreement with its disordered nature. Values plotted in Fig. 4 were color coded according to the residue number in order to facilitate interpretation of the data. The most flexible residue is C-terminal K 173, with dynamics limited to sub-nanosecond motions, followed by somewhat slower E 170, Y 165 and D 167. The trend continues with a cluster of residues E 135–D 159 exhibiting a very similar motional behavior. A distinct cluster of spectral density values is observed for residues D 85–E 129, apparently more influenced by slower molecular motions. Interestingly, the region D 85–E 129 contains a unique positively charged sequence KAKKKKAKK between K 96 and K 104. A recent study utilizing paramagnetic relaxation enhancement (Papoušková et al. 2013) revealed that the lysine stretch makes transient contacts with various regions of the strongly acidic C-terminal domain (72 % residues between E 107 and E 171 are aspartic or glutamic acid). Such contacts may explain the higher rigidity of residues in the vicinity of the lysine stretch.

As mentioned above, contributions of motions on the microsecond-to-millisecond timescale were effectively suppressed in the R_2 experiment with the 180° pulses in the relaxation period separated by 0.9 ms. On the other hand, the relaxation-dispersion CPMG experiment, discussed above, showed that the C-terminal domain is not completely free of the slow exchange (Fig. 5). The exchange contribution was very small for Y 165, D 167, E 170, and K 173. All other residues studied by spectral density mapping

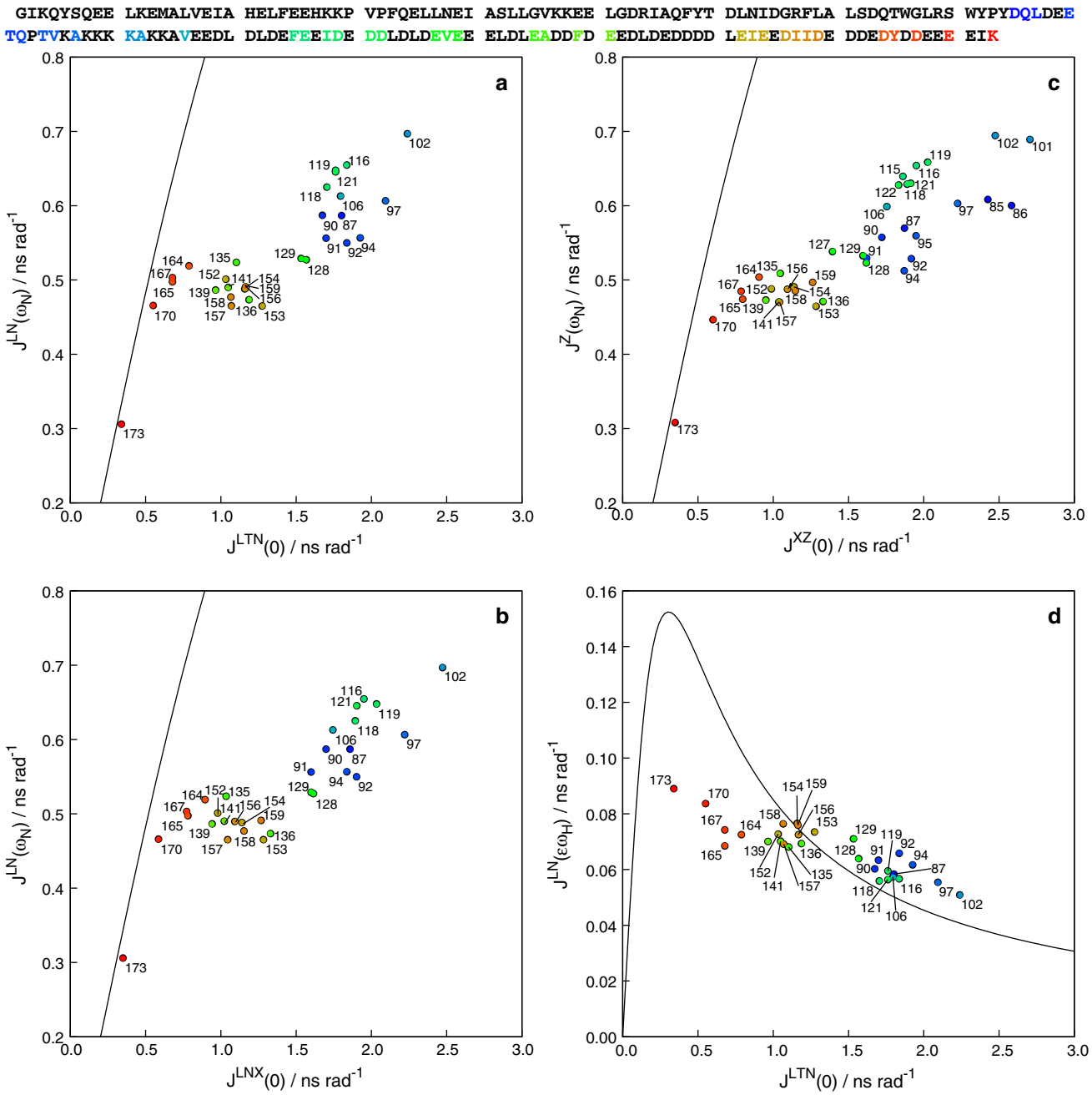

Fig. 4 $J^{LTN}(0)$ versus $J^{LN}(\omega_N)$ **(a)**, $J^{LNX}(0)$ vs. $J^{LN}(\omega_N)$ **(b)**, $J^{XZ}(0)$ vs. $J^{Z}(\omega_N)$ **(c)**, and $J^{LTN}(0)$ versus $J^{LN}(\varepsilon\omega_H)$ **(d)** for the disordered region of the δ-subunit of RNA polymerase (Y 84–K 173, note that the sequence starts at G 2 because M 1 is cleaved off by the bacterial expression system). The plotted values were calculated from data acquired at the 600 MHz spectrometer. Data are *color-coded* according to the residue number. The *colors* correspond to the *colors* of letters in the sequence displayed above the plots. Standard deviations of $J^{LTN}(0)$, $J^{LNX}(0)$, $J^{XZ}(0)$, $J^{LN}(\omega_N)$, $J^{Z}(\omega_N)$, and $J^{LN}(\varepsilon\omega_H)$ did not exceed 1.7, 1.0, 1.0, 0.7, 1.2, and 2.6 %, respectively, and are not presented for the sake of clarity (note that the standard deviations are displayed in Supplementary Material, Fig. S2)

exhibited a small, but significant slow exchange. The slow exchange may indicate that the amide proton exchange is not completely suppressed at pH 6.6 and 27°C (Kim et al. 2013). However, the fact that the slow exchange was not observed for the most exposed C-terminal residues supports another interpretation, i.e., that the exchange contribution is related to conformational changes of the C-terminal domain.

In order to document the possibility to detect the slow exchange by spectral density mapping, the R_2 experiment was repeated with a longer delay of the 180° pulses in the relaxation period, 1.4 ms.

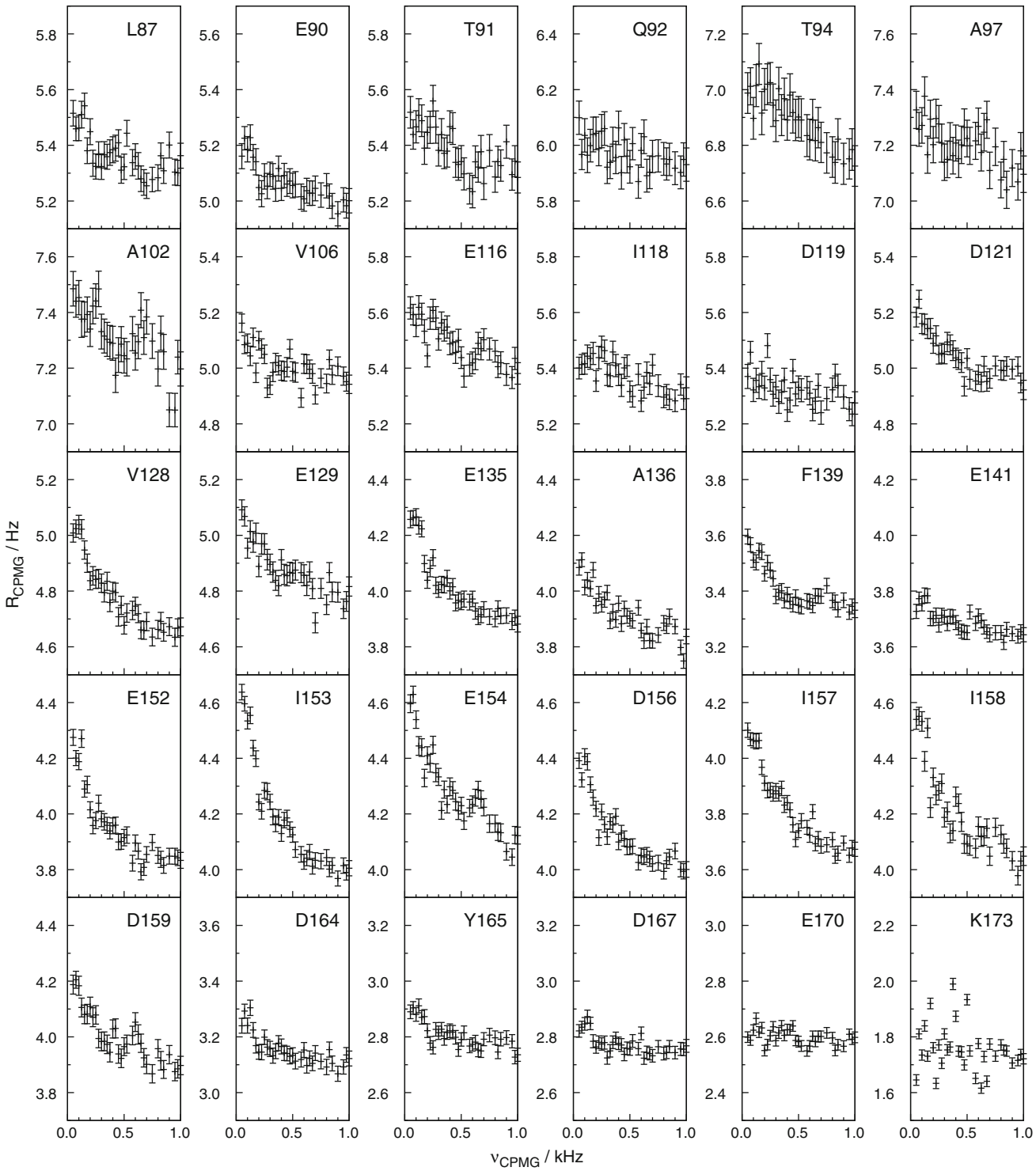

Fig. 5 Results of the CPMG relaxation dispersion experiments for the residues of the disordered region of the δ-subunit of RNA polymerase from *Bacillus subtilis* whose resolution allowed spectral density mapping at 500 and 600 MHz spectrometers. Values of the apparent relaxation rate measured at the 600 MHz spectrometer are plotted as a function of the frequency of the 180° pulses applied during the CPMG sequence

Comparison of the $J^{\mathrm{LTN}}(0)$ values obtained at two different CPMG frequencies revealed small exchange contributions also for residues in the disordered domain (Fig. 3). The exchange was most obvious for I 153, E 154, and I 158, in agreement with the relaxation dispersion data (Fig. 5).

Conclusion

Spectral density mapping allows one to describe molecular motions without defining the number of motional modes and making assumptions of their independence. It is particularly useful when the model-free approach cannot be used, e.g. for disordered proteins and other flexible molecules.

The proposed methods extend applicability of the spectral density mapping to cases that could not be studied by the original protocol accurately. The optimized LTN protocol provides accurate low- and high-frequency spectral density values, free of the contribution of the slow exchange. LNX complements the data with an exchange-free zero-frequency value. XZ represents an alternative protocol of exchange-free spectral density mapping, that is most exact but also most demanding experimentally. Finally, LTX offers a possibility to analyze relaxation rates in the absence of NOE and serves as a better indicator of slow dynamics than LTN.

The case study showed that the original spectral density mapping approach (LTN) is well suited for analysis of ^{15}N relaxation of backbone amide in well-ordered proteins. Favorable relaxation properties of the disordered domain allowed us to apply all spectral density mapping protocols with high precision and to assess possible systematic errors of the obtained data. Values obtained by using different approaches were consistent. Cross-correlated relaxation allowed for determination of exchange-free $J(0)$. In principle, results of the presented methods might be compromised by the orientational bias, which is difficult to predict in the case of intrinsically disordered proteins, when a structural model is not available. However, analysis of the calculated spectral density values showed that this source of a systematic error is unlikely to be significant, at least for the molecule studied in this work.

Acknowledgments This work was supported by the Czech Science Foundation, grant number GA 13-16842S (P. K., A. R., L. K., L. Ž). The partial support by the project "CEITEC—Central European Institute of Technology" from European Regional Development Fund, grant number CZ.1.05/1.1.00/02.0068, and the Joint Research Activity of the 7th Framework program of the EC (BioNMR, no. 261863) is also acknowledged.

References

Barthe P, Chiche L, Declerck N, Delsuc M, Lefèvre J, Malliavin T, Mispelter J, Stern M, Lhoste J, Roumestand C (1999) Refined solution structure and backbone dynamics of ^{15}N-labeled C12A-p8^{MTCP1} studied by NMR relaxation. J Biomol NMR 15:271–288. doi:10.1023/A:1008336418418

Bussell R, Eliezer D (2001) Residual structure and dynamics in Parkinson's disease-associated mutants of alpha-synuclein. J Biol Chem 276(49):45,996–46,003

Cao W, Bracken C, Kallenbach NR, Lu M (2004) Helix formation and the unfolded state of a 52-residue helical protein. Protein Sci 13:177–189. doi:10.1110/ps.03383004

d'Auvergne EJ, Gooley PR (2008) Optimisation of NMR dynamic models I. Minimisation algorithms and their performance within the model-free and Brownian rotational diffusion spaces. J Biomol NMR 40:107–119. doi:10.1007/s10858-007-9214-2

d'Auvergne EJ, Gooley PR (2008) Optimisation of NMR dynamic models II. A new methodology for the dual optimisation of the model-free parameters and the Brownian rotational diffusion tensor. J Biomol NMR 40:121–133. doi:10.1007/s10858-007-9213-3

Delaglio F, Grzesiek S, Vuister G, Zhu G, Pfeifer J, Bax A (1995) NMRPipe—a multidimensional spectral processing system based on UNIX pipes. J Biomol NMR 6:277–293. doi:10.1007/BF00197809

DeSaro F, Woody A, Helmann J (1995) Structural-analysis of the *Bacillus-subtilis* delta-factor—a protein polyanion which displaces RNA from RNA-polymerase. J Mol Biol 252(2):189–202

Dyson H, Wright P (2004) Unfolded proteins and protein folding studied by NMR. Chem Rev 104(8):3607–3622

Eliezer D (2007) Characterizing residual structure in disordered protein states using nuclear magnetic resonance. Methods Mol Biol 350:49–67

Eliezer D (2009) Biophysical characterization of intrinsically disordered proteins. Curr Opin Struct Biol 19(1):23–30

Farrow N, Zhang O, Szabo A, Torchia D, Kay L (1995) Spectral density function mapping using ^{15}N relaxation data exclusively. J Biomol NMR 6:153–162

Farrow NA, Zhang OW, FormanKay JD, Kay LE (1997) Characterization of the backbone dynamics of folded and denatured states of an SH3 domain. Biochemistry 36:2390–2402. doi:10.1021/bi962548h

Ferrage F, Cowburn D, Ghose R (2009) Accurate sampling of high-frequency motions in proteins by steady-state ^{15}N–^{1}H nuclear Overhauser effect measurements in the presence of cross-correlated relaxation. J Am Chem Soc 131(17):6048+. doi:10.1021/ja809526q

Hall J, Fushman D (2003) Direct measurement of the transverse and longitudinal ^{15}N chemical shift anisotropy-dipolar cross-correlation rate constants using ^{1}H-coupled HSQC spectra. Magn Reson Chem 41:837–842. doi:10.1002/mrc.1253

Hall J, Dayie K, Fushman D (2003) Direct measurement of the ^{15}N CSA/dipolar relaxation interference from coupled HSQC spectra. J Biomol NMR 26:181–186. doi:10.1023/A:1023546107553

Halle B, Andersson T, Forsén S, Lindman B (1981) Protein hydration from water oxygen-17 magnetic-relaxation. J Am Chem Soc 103:500–508. doi:10.1021/ja00393a004

Ishima R, Nagayama K (1995) protein backbone dynamics revealed by quasi spectral density function analysis of amide N-15 nuclei. Biochemistry 34:3162–3171. doi:10.1021/bi00010a005

Ishima R, Nagayama K (1995) Quasi-spectral-density function analysis for nitrogen-15 nuclei in proteins. J Magn Reson Ser B 108:73–76. doi:10.1006/jmrb.1995.1104

Kim S, Wu KP, Baum J (2013) Fast hydrogen exchange affects ^{15}N relaxation measurements in intrinsically disordered proteins. J Biomol NMR 55:249–256. doi:10.1007/s10858-013-9706-1

Korzhnev D, Billeter M, Arseniev A, Orekhov V (2001) NMR studies of Brownian tumbling and internal motions in proteins. Prog Nucl Magn Reson Spectrosc 38:197–266. doi:10.1016/S0079-6565(00)00028-5

Křížová H, Žídek L, Stone M, Novotný M, Sklenář V (2004) Temperature-dependent spectral density analysis applied to monitoring backbone dynamics of major urinary protein-I complexed with the pheromone 2-sec-butyl-4,5-dihydrothiazole.

J Biomol NMR 28:369–384. doi:10.1023/B:JNMR.0000015404.61574.65

Lefèvre J, Dayie K, Peng J, Wagner G (1996) Internal mobility in the partially folded DNA binding and dimerization domains of GAL4: NMR analysis of the N–H spectral density functions. Biochemistry 35:2674–2686. doi:10.1021/bi9526802

Lipari G, Szabo A (1982) Model-free approach to the interpretation of nuclear magnetic-resonance relaxation in macromolecules. 1. Theory and range of validity. J Am Chem Soc 104:4546–4559. doi:10.1021/ja00381a009

Lipari G, Szabo A (1982) Model-free approach to the interpretation of nuclear magnetic-resonance relaxation in macromolecules. 2. Analysis of experimental results. J Am Chem Soc 104:4559–4570. doi:10.1021/ja00381a010

Long D, Liu M, Yang D (2008) Accurately probing slow motions on millisecond timescales with a robust NMR relaxation experiment. J Am Chem Soc 130(8):2432–2433. doi:10.1021/ja710477h

Motáčková V, Nováček J, Zawadzka-Kazimierczuk A, Kazimierczuk K, Žídek L, Šanderová H, Krásný L, Koźmiński W, Sklenář V (2010) Strategy for complete NMR assignment of disordered proteins with highly repetitive sequences based on resolution-enhanced 5D experiments. J Biomol NMR 48(3):169–177. doi:10.1007/s10858-010-9447-3

Motáčková V, Šanderová H, Žídek L, Nováček J, Padrta P, Švenková A, Korelusová J, Jonák J, Krásný L, Sklenář V (2010) Solution structure of the N-terminal domain of *Bacillus subtilis* δ subunit of RNA polymerase and its classification based on structural homologs. Proteins 78(7):1807–1810. doi:10.1002/prot.22708

Ochsenbein F, Guerois R, Neumann JM, Sanson A, Guittet E, van Heijenoort C (2001) ^{15}N NMR relaxation as a probe for helical intrinsic propensity: The case of the unfolded D2 domain of annexin I. J Biomol NMR 19:3–18. doi:10.1023/A:1008390606077

Papoušková V, Kadeřávek P, Otrusinová O, Rabatinová A, Šanderová H, Nováček J, Krásný L, Sklenář V, Žídek L (2013) Structural study of the partially disordered full-length δ subunit of RNA polymerase from *Bacillus subtilis*. ChemBioChem 14:1772–1779. doi:10.1002/cbic.201300226

Pelupessy P, Espallargas GM, Bodenhausen G (2003) Symmetrical reconversion: measuring cross-correlation rates with enhanced accuracy. J Magn Res 161:258–264. doi:10.1016/S1090-7807(02)00190-8

Pelupessy P, Ferrage F, Bodenhausen G (2007) Accurate measurement of longitudinal cross-relaxation rates in nuclear magnetic resonance. J Chem Phys 126. doi:10.1063/1.2715583

Peng J, Wagner G (1992) Mapping of spectral density-functions using heteronuclear NMR relaxation measurements. J Magn Reson 98:308–332. doi:10.1016/0022-2364(92)90135-T

Peng J, Wagner G (1992) Mapping of the spectral densities of N–H bond motions in eglin *c* using heteronuclear relaxation experiments. Biochemistry 31:8571–8586. doi:10.1021/bi00151a027

Pero J, Nelson J, Fox TD (1975) Highly asymmetric transcription by rna-polymerase containing phage-Sp01-induced polypeptides and a new host protein. Proc Natl Acad Sci USA 72:1589–1593. doi:10.1073/pnas.72.4.1589

Rabatinová A, Šanderová H, Jirát Matějčková J, Korelusová J, Sojka L, Barvík I, Papoušková V, Sklenář V, Žídek L, Krásný L (2013) The delta subunit of RNA polymerase is required for rapid changes in gene expression and competitive fitness of the cell. J Bacteriol 195:2603–2611. doi:10.1128/JB.00188-13

Redfield A (1965) The theory of relaxation processes. Adv Magn Reson 1:1–32

Tjandra N, Wingfield P, Stahl S, Bax A (1996) Anisotropic rotational diffusion of perdeuterated HIV protease from ^{15}N NMR relaxation measurements at two magnetic fields. J Biomol NMR 8:273–284. doi:10.1007/BF00410326

Tompa P (2012) Intrinsically disordered proteins: a 10-year recap. Trends Biochem Sci 37:509–516. doi:10.1016/j.tibs.2012.08.004

Uversky VN (2013) Unusual biophysics of intrinsically disordered proteins. Biochim Biophys Acta 1834:932–951. doi:10.1016/j.bbapap.2012.12.008

Wangsness R, Bloch F (1953) The dynamical theory of nuclear induction. Phys Rev Lett 89(4):728–739. doi:10.1103/PhysRev.89.728

Yao J, Chung J, Eliezer D, Wright PE, Dyson HJ (2001) NMR structural and dynamic characterization of the acid-unfolded state of apomyoglobin provides insights into the early events in protein folding. Biochemistry 40:3561–3571. doi:10.1021/bi002776i

Yao L, Grishaev A, Cornilescu G, Bax A (2010) Site-specific backbone amide ^{15}N chemical shift anisotropy tensors in a small protein from liquid crystal and cross-correlated relaxation measurements. J Am Chem Soc 132:4295–4309. doi:10.1021/ja910186u

Zhang XC, Xu YQ, Zhang JH, Wu JH, Shi YY (2005) Structural and dynamic characterization of the acid-unfolded state of hUBF HMG box 1 provides clues for the early events in protein folding. Biochemistry 44:8117–8125. doi:10.1021/bi0501939